ACS APPLIED ENERGY MATERIALS

www.acsaem.org Article

Multiple Network Binders via Dual Cross-Linking for Silicon Anodes of Lithium-Ion Batteries

Xingxing Jiao,[‖] Xiaodong Yuan,[‖] Jianqing Yin, Farshad Boorboor Ajdari, Yangyang Feng,* Guoxin Gao, and Jiangxuan Song*

Cite This: https://doi.org/10.1021/acsaem.1c02231 Read Online

ACCESS | Metrics & More | Article Recommendations | Supporting Information

ABSTRACT: Silicon has attracted much attention as a promising anode material in lithium-ion batteries owing to its high specific capacity. However, silicon anode suffers large volume expansion during periodical lithiation/delithiation processes, leading to particle pulverization and thus electrochemical performance degradation. Herein, we report a water-soluble three-dimensional network polymer binder for silicon anode in which the introduced poly(ethylene glycol) and divalent cation Ca^{2+} can form chemical cross-linking and physical cross-linking with poly(acrylic acid), respectively. Poly(ethylene glycol) serves as a soft segment to regulate the mechanical properties of the polymer, and the divalent cation Ca^{2+} acts as a physical cross-linking agent to form a dual network with poly(acrylic acid). The multiple network binder owns good mechanical strength, strain resistance ability, and strong adhesion with Si particles and Cu collector, thereby preserving the stability of the silicon electrode. Therefore, silicon anode with this rationally designed binder exhibits excellent electrochemical performance with a discharge capacity of 1596 mAh/g after 800 cycles at a current density of 2 A/g. This design can provide a way to alleviate the volume expansion of the silicon anode and other high-capacity alloy anodes with large volume change for advanced batteries.

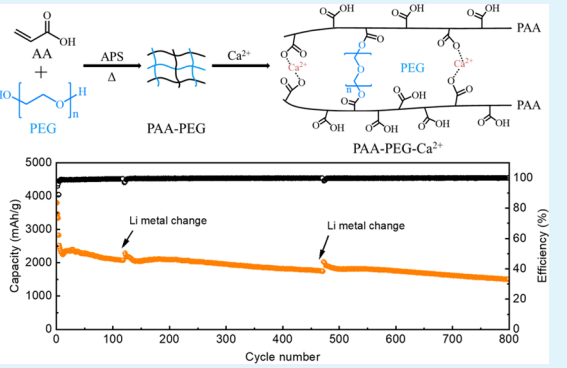

KEYWORDS: *lithium-ion batteries, silicon anode, binder, water-soluble polymer, dual cross-linking network*

1. INTRODUCTION

Lithium-ion batteries (LIBs), regarded as one of the most promising energy storage devices, have been widely applied in various fields in the flourishing human society.[1−5] However, the development of LIBs has been strangled by the limited energy density caused by the commercial graphite anode of 372 mAh/g. Impressively, silicon (Si) possesses an ultrahigh specific capacity of ∼4200 mAh/g and a low electrochemical potential of ∼0.4 V versus Li/Li^+, which is deemed as the promising anodic material to pursue high energy density (>350 Wh/kg).[6−9]

Despite these advantages, the performance of the Si anode has been critically hindered by the overlarge volume expansion during the lithiation process. It results in the pulverization of electrodes and uncontrolled growth of the solid electrolyte interphase (SEI).[10−13] Furthermore, the volume change is in direct agreement with the rapid capacity fading, and the Coulombic efficiency decreases. Briefly, solving the overlarge volume change is the crucial point for the practical utilization of Si anode in high-energy-density batteries. Regarding the significant volume change of Si, there have been numerous endeavors lately,[14−18] including low-dimensional structures (nanoparticles,[19−22] nanowires,[23,24] nanotubes,[25,26] and nanoscale thin films[27,28]) and multistage structures (porous Si[29,30] and core−shell structures[31−33]). The nanostructure design of the Si-based anodes allows them to more effectively handle the huge volume change and improve the cyclic stability to some extent. However, the current approaches cannot tackle the pulverization of active materials and collapse of the electrode, resulting from continuous volume changes in Si particles.[34,35]

As reported previously, polymer binder is a vital segment in Si-based electrodes to maintain electrode integrity. Poly(vinylidene fluoride) (PVDF) is widely employed in traditional LIBs due to its good thermal and electrochemical stability. However, due to a poor interaction between the binder and Si particles with a weak van der Waals force, PVDF cannot efficiently accommodate the volume change of the Si electrode during cycling.[13,36,37] Furthermore, poly(acrylic acid) (PAA),[38] carboxy-methyl cellulose (CMC),[39] and alginate have been developed to improve the cyclic life by maintaining Si-based anode integrity.

Received: July 27, 2021
Accepted: August 17, 2021

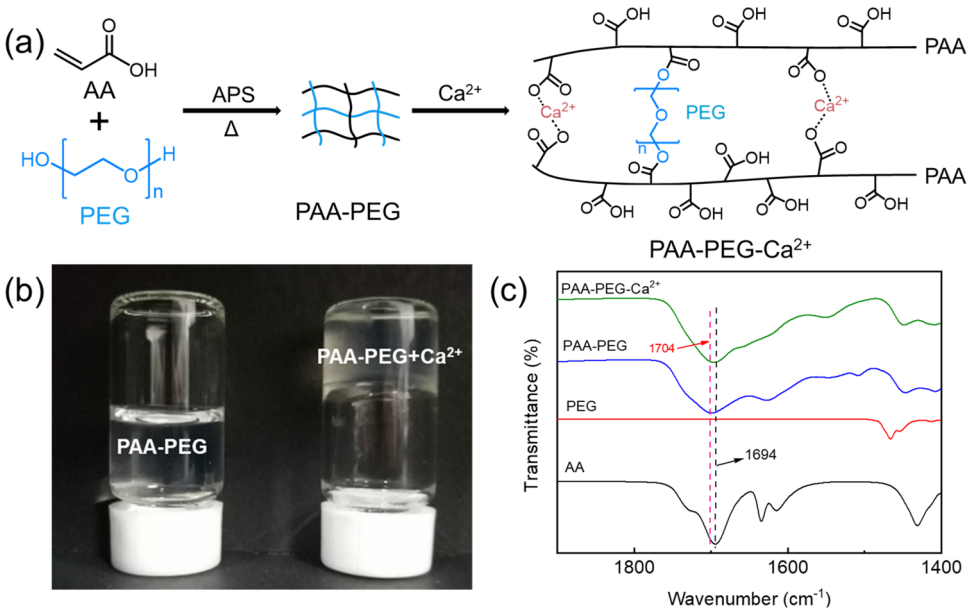

Figure 1. (a) Synthetic process of PAA-PEG-Ca^{2+} binder. (b) Digital photographs of the PAA-PEG and PAA-PEG-Ca^{2+} binders. (c) FTIR spectra of AA, PEG, PAA-PEG, and PAA-PEG-Ca^{2+} binders.

The linear polymer binders with functional groups can strengthen the adhesion with Si particles by forming hydrogen bonds or covalent chemical bonds on the Si particle surface and diminishing the electrode splitting. However, their chains are exposed to deterioration with repeated expansion/shrinkage of Si particles during the lithiation and delithiation processes. Incorporating a cross-linked polymer matrix protects polymer chains from irreversible slippage and contributes to the integrity of Si-based anodes.[40−43]

Recently, Song et al. reported an interpenetrated gel polymer binder (PAA−PVA)[44] for Si anodes through a simple in situ thermal cross-linking technology, which formed a deformable polymer network and strong binding with Si, resulting in enhanced cycling stability and Coulombic efficiency. Liu et al. designed a three-dimensional (3D) network composite binder through interweaving hard PFA and soft PVA.[45] The combination of hard and soft polymers enabled a high areal capacity and long cycling performance. Moreover, Cao and coauthors designed a functional polymer network (CS-CG + GA) by tuning the grafting density and the degree of cross-linking density, and the SiNP-based electrode with the binder exhibited an excellent cycling performance.[46] Therefore, the development of a new multifunctional cross-linking binder is conducive to buffering the inherent volume change of silicon anodes in LIBs during repeated lithiation/delithiation processes.

Herein, we designed a three-dimensional (3D) network binder in which PAA was cross-linked with poly(ethylene glycol) (PEG) and calcium ion (Ca^{2+}) to form chemical and physical cross-linking, respectively. PAA with plenty of carboxyl groups can provide strong adhesion with Si particles, and the introduced PEG and Ca^{2+} can tune the mechanical property of the binder. The 3D network PAA-PEG-Ca^{2+} polymer binder embraces the dual cross-linked structure, delivering sufficient mechanical strength to maintain the integrity of Si anode and improving the cyclic performance.

2. EXPERIMENTAL SECTION

2.1. Materials. Acrylic acid (AA) was purchased from Chengdu Xiya Reagent Co., Ltd. (Chengdu, China). Poly(ethylene glycol) (PEG, MW = ∼5000) and ammonium persulfate (99.99%) were purchased from Aladdin Bio-Chem Technology Co., Ltd. (Shanghai, China). SiNP with an average diameter of 100 nm was purchased from Zhejiang Zhongning Polysilicon Co., Ltd. Calcium chloride (≥96%) was purchased from Sinopharm Chemical Reagent Co., Ltd. All reagents were used without further purification.

2.2. Characterization. Attenuated total reflectance Fourier transform infrared spectroscopy (ATR FTIR) was performed on a Bruker Alpha II spectrometer, and the samples of PAA-PEG and PAA-PEG-Ca^{2+} were prepared at 120 °C for 3 h. A field-emission scanning electron microscope (FESEM; Gemini SEM 500) was used to examine the morphology of the samples. The size of Si particles was tested on the Brunauer−Emmett−Teller (BET) surface area (Micromeritics ASAP 2460). For mechanical and peeling tests of PAA and PAA-PEG-Ca^{2+} polymers, an electronic universal testing machine (UTM-2502) was utilized.

2.3. Polymer Synthesis. Preparation of PAA-PEG-Ca^{2+} binder: The interpenetrating network polymer of PAA-PEG was synthesized using a free-radical polymerization method. AA (3.6 g) dissolved in deionized water (6 mL) and ammonium persulfate (0.5 wt % of the monomer mass) as initiators was added into a glass vessel equipped with a mechanical stirrer in an oil bath. When the reactor was heated to 80 °C, PEG (0.44 g) dissolved in deionized water (8 mL). After stirring for 60 min under these conditions, the PAA-PEG polymer was obtained. Then, the PAA-PEG-Ca^{2+} was synthesized by adding different weight ratios of $CaCl_2$ into the PAA-PEG solutions and stirred for 30 min in which the Ca^{2+} was used to form physical cross-linking with PAA.

2.4. Preparation of Si Electrodes and Electrochemical Measurements. For the PAA-PEG-Ca^{2+} electrodes, the slurry was made by uniformly mixing the Si nanoparticles (SiNP), Super P carbon black, and PAA-PEG-Ca^{2+} binder with the weight ratio of 70:15:15, and then coated on a copper foil and dried in a vacuum oven at 120 °C for 3 h. The control samples of PAA-PEG and PAA-SiNP electrodes were obtained in the same way. Coin-type (CR2032) half-cells, using 1 M $LiPF_6$ in ethylene carbonate (EC)−diethyl carbonate (DEC) (1:1, volume ratio) containing 10 vol % fluoroethylene carbonate (FEC) as the electrolyte and Li foil as the counter electrode, were assembled in an argon-filled glovebox with oxygen and water content lower than 0.1 ppm. The areal mass loading

https://doi.org/10.1021/acsaem.1c02231
ACS Appl. Energy Mater. XXXX, XXX, XXX−XXX

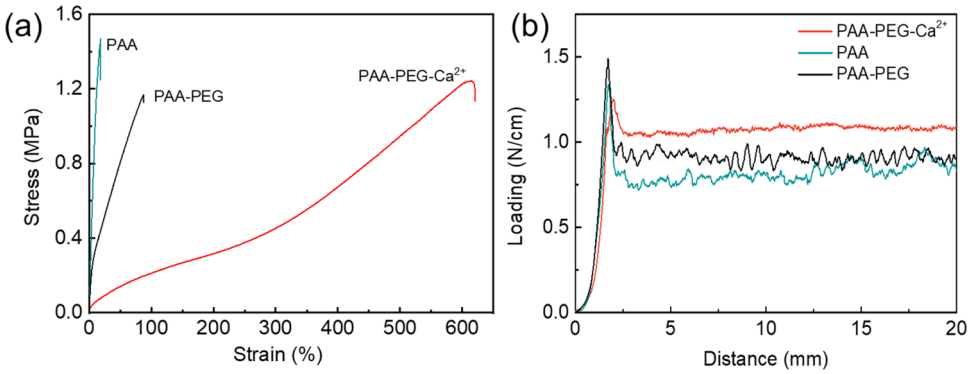

Figure 2. (a) Stress−strain curves of the PAA binder, PAA-PEG binder, and PAA-PEG-Ca^{2+} binder. (b) 180° peeling test results of Si electrodes based on PAA-PEG-Ca^{2+}, PAA-PEG, and PAA binders.

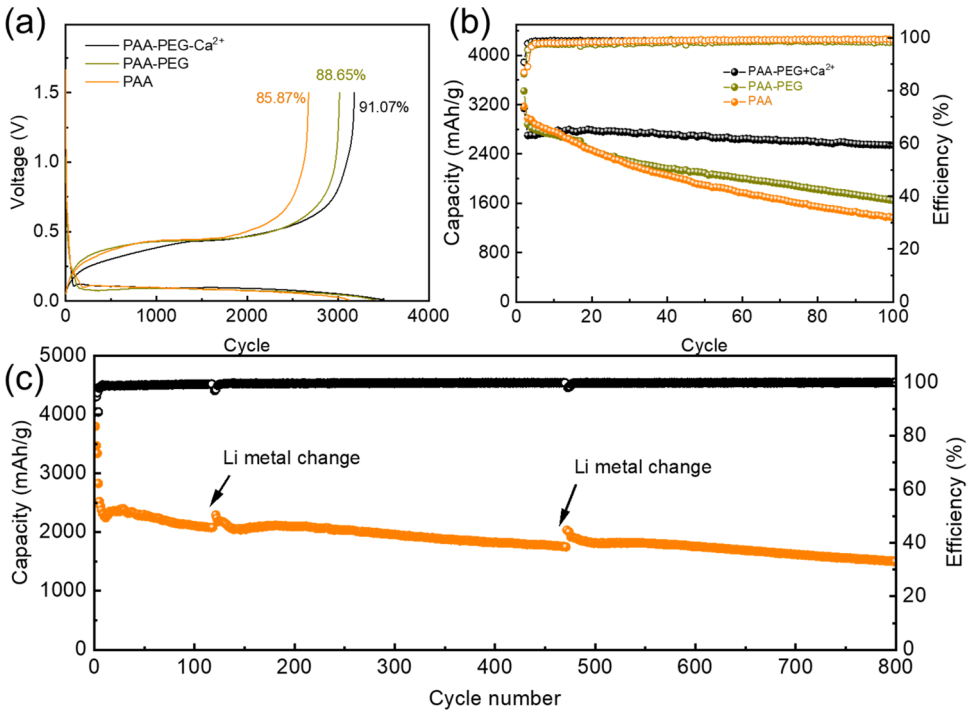

Figure 3. Electrochemical performances of SiNP electrodes, including PAA-PEG-Ca^{2+}, PAA-PEG, and PAA as binders. (a) First charge−discharge profiles were measured at 0.2 A/g. (b) Discharging capacity and Coulombic efficiency measured at 1.2 A/g. (c) Discharging capacity and Coulombic efficiency cycled at 2 A/g.

of Si was about 0.7 mg/cm^2. The galvanostatic charge/discharge was carried out between 0.01 and 1.5 V versus Li/Li^+ at 0.05C for the precycle, and then 0.3C (1.2 A/g) or 0.5C (2 A/g) was applied for the subsequent cycles on a Land battery tester. The cyclic voltammetry (CV) plot was recorded by the CHI1000C electrochemical workstation at a scan rate of 0.05 mV/s. All specific capacities and current densities were calculated on the weight of Si.

3. RESULTS AND DISCUSSION

The synthetic process of the 3D network PAA-PEG-Ca^{2+} polymer binder is shown in Figure 1a. The interpenetrating network PAA-PEG polymer was prepared via free-radical polymerization using 90 wt % acrylic acid (AA) in 10 wt % PEG water solution in which PAA owns the sturdy framework role and PEG is selected as a soft segment to adjust the mechanical property. Compared with the PAA-PEG polymer, the introduction of Ca^{2+} in the PAA-PEG solution can form the gel polymer by the physical connection between Ca^{2+} and abundant carboxylic hydroxyl of PAA (Figure 1b). Furthermore, PAA and PEG can form chemical bonds via thermal cross-linking between carboxyl groups in PAA and hydroxy groups in PEG. Plenty of hydrogen bonds in the PAA chains can also provide strong adhesion with Si particles and the copper collector. Therefore, it is reasonable to expect that the PAA-PEG-Ca^{2+} binder can enhance the cyclic performance of the Si anode.

Fourier transform infrared (FTIR) spectroscopy was conducted to identify the structure of the PAA-PEG-Ca^{2+} binder. Figures 1c and S1 illustrate that the peaks in the spectrum of AA centered at 1694 and 3000 cm^{-1} are due to −COOH groups.[47,48] The peak centered at 1704 cm^{-1} in the PAA-PEG spectrum, ascribed to the ester group (−COO−),[44] also consisted of the PAA-PEG-Ca^{2+} binder. Thus, the results indicate that the PAA-PEG-Ca^{2+} polymer binder is successfully prepared.

As discussed above, the PAA-PEG-Ca^{2+} polymer binder is expected to embrace excellent mechanical properties, con-

https://doi.org/10.1021/acsaem.1c02231
ACS Appl. Energy Mater. XXXX, XXX, XXX−XXX

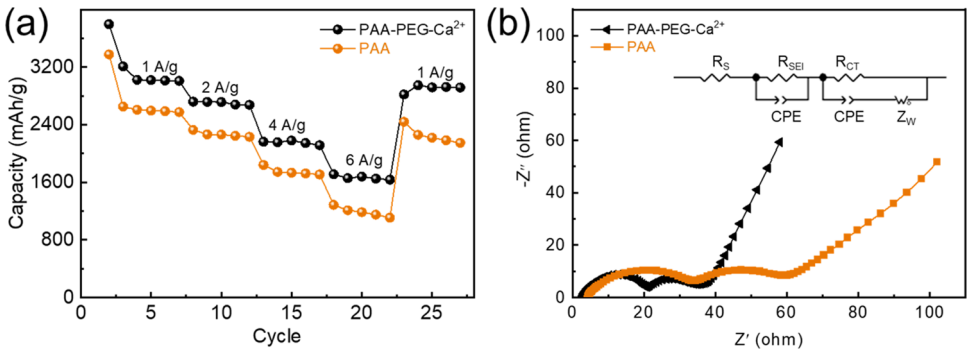

Figure 4. (a) Rate performance of PAA-PEG-Ca^{2+}-SiNP and PAA-SiNP electrodes. (b) Nyquist plots of PAA-PEG-Ca^{2+}-SiNP and PAA-SiNP electrodes after 10 cycles.

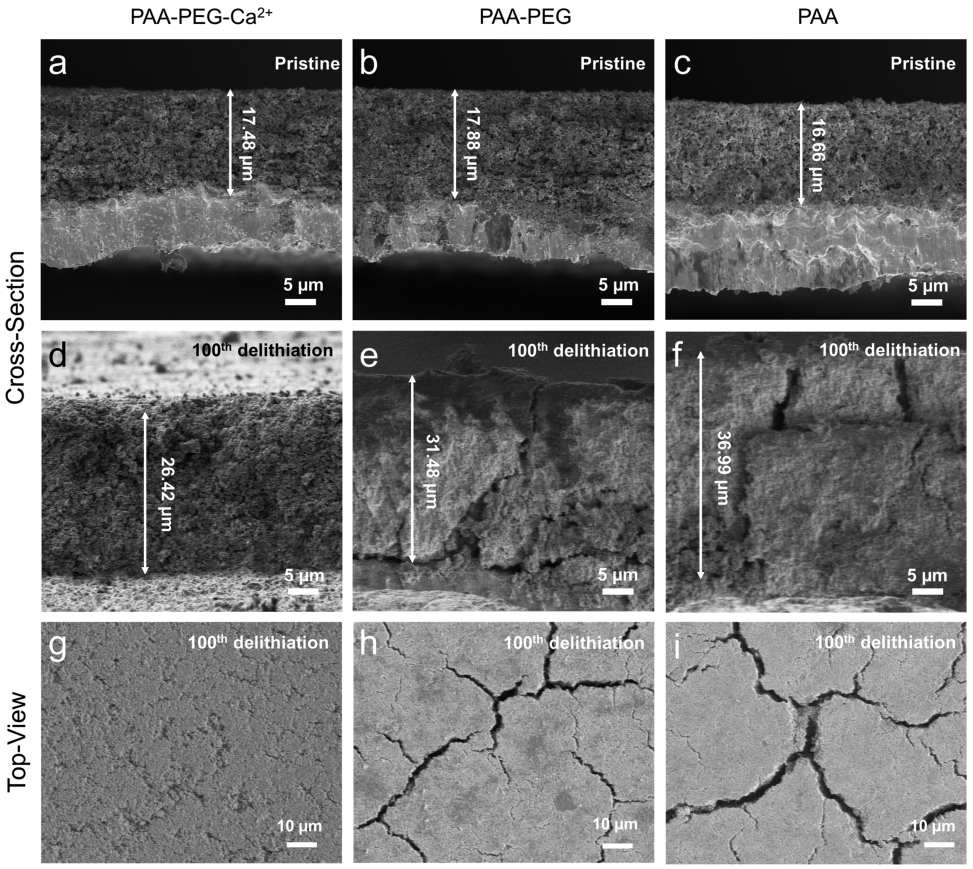

Figure 5. Ex situ SEM characterization of SiNP electrodes based on PAA-PEG-Ca^{2+}, PAA-PEG, and PAA binders before and after cycling. (a–c) Cross-sectional images of (a) PAA-PEG-Ca^{2+}-SiNP, (b) PAA-PEG-SiNP, and (c) PAA-SiNP electrodes before cycling. (d–f) Cross-sectional images of (d) PAA-PEG-Ca^{2+}-SiNP, (e) PAA-PEG-SiNP, and (f) PAA-SiNP electrodes after the 100th delithiation. (g–i) Top-view SEM images of (g) PAA-PEG-Ca^{2+}-SiNP, (h) PAA-PEG-SiNP, and (i) PAA-SiNP electrodes after the 100th delithiation.

firmed by the stress–strain and peeling test. As shown in Figure 2a, PAA film displays a nearly linear large-slope stress–strain curve, and its rupture occurs with 15% strain, illustrating the low elastic deformation of the PAA polymer. On the contrary, the PAA-PEG-Ca^{2+} film exhibits a stress–strain curve with a maximum tensile strength of up to 1.24 MPa and 600% stretching. Furthermore, the 180° peeling test was conducted to evaluate the adhesion of the binder to Si particles and Cu collector, which came from the different structures inside the polymer binders. As shown in Figure 2b, it is evident that the electrodes with PAA and PAA-PEG binders show weaker adhesion (0.8 and 0.9 N/cm, respectively) compared with that of PAA-PEG-Ca^{2+} binder, implying that the PAA and PAA-PEG can adhere to Si particles by covalent bonding or hydrogen bonding. However, the PAA-PEG-Ca^{2+}-SiNP electrode displays improved adhesion with a value of 1.1 N/cm, attributed to the formation of multiple networks with abundant hydrogen bonds with Si particles.

The electrochemical performance of Si anodes with the binders was evaluated with CR2032-type coin cell using Li foil as the counter electrode. The electrode was fabricated using SiNPs (mean size of ~100 nm in Figure S2), binder, and super P with a weight ratio of 70:15:15. In the first cycle, the initial lithium insertion process occurs together with the decomposition of the electrolyte and subsequent formation of SEI. The electrode with PAA-PEG-Ca^{2+} displays a higher reversible

https://doi.org/10.1021/acsaem.1c02231
ACS Appl. Energy Mater. XXXX, XXX, XXX–XXX

Table 1. Comparative Electrochemical Performance of SiNP Electrodes with Different Binders

binder	active materials	initial Coulombic efficiency (ICE) (%)	cycling performance	ref
PAA-PEG-Ca^{2+}	SiNP	91.1	1596 mAh/g (2000 mA/g, 800 cycles)	this work
Alg-PAA	SiNP	86.8	945 mAh/g (200 mA/g, 110 cycles)	51
CS-PAA	SiNP	87.4	1243 mAh/g (420 mA/g, 100 cycles)	52
PAA-CMC	SiNP	88.0	2000 mAh/g (300 mA/g, 100 cycles)	53
PAA-pullan	SiNP	84.0	1400 mAh/g (1500 mA/g, 200 cycles)	54
PAANa-g-CMC	SiNP	84.0	1816 mAh/g (840 mA/g, 100 cycles)	55
PAA-PEGPBI	SiNP		1221 mAh/g (1000 mA/g, 50 cycles)	56
PDA-PAA-PEO	SiNP	74.0	1597 mAh/g (2000 mA/g, 200 cycles)	57
Alg-C-CS	SiNP	74.5	750 mAh/g (100 mA/g, 100 cycles)	58
β-CDp-6AD	SiNP	84.0	1450 mAh/g (2000 mA/g, 150 cycles)	59

capacity of 3491.1 mAh/g with an initial Coulombic efficiency of 91.07% at a current density of 0.2 A/g, which is higher than that of electrodes with PAA-PEG-SiNP (88.65%) and PAA-SiNP (85.87%) (Figure 3a). This is because the SiNP electrode with a 3D network PAA-PEG-Ca^{2+} binder maintains a stable electrode structure (less cracks and newly formed fresh surface) and thus mitigates excessive electrolyte decomposition. The cycling voltammetry of the PAA-PEG-Ca^{2+}-SiNP, PAA-PEG-SiNP, and PAA-SiNP electrodes was tested at a scanning rate of 0.05 mV/s to detect the redox peak of active material (Figure S3), which is consistent with the reported literature studies.[49] Several electrodes with different PAA-PEG-Ca^{2+} binders were prepared to optimize the ratio of PAA/Ca^{2+} (Figure S4). The electrode with PAA-PEG-Ca^{2+} exhibits excellent cycling stability with almost no capacity attenuation after 100 cycles at the current density of 1.2 A/g, which also displays better cyclic performance than the PAA-SiNP electrode (Figure 3b). Impressively, the SiNP electrode with the PAA-PEG-Ca^{2+} polymer binder exhibits an outstanding cyclic performance with a discharge capacity of 1596 mAh/g after 800 cycles at a current density of 2 A/g (Figure 3c). To exclude the effect of dendritic issues of the Li metal electrode shown in Figure S5 and assure that the cyclic performance is intimated with properties of PAA-PEG-Ca^{2+}, a fresh Li metal electrode was replaced at 130th and 480th cycles.

As shown in Figure 4a, the Si electrode with PAA-PEG-Ca^{2+} binder embraces the improved rate performance compared with that of the PAA binder, which delivers 3024, 2720, 2163, and 1712 mAh/g at current densities of 1, 2, 4, and 6 A/g, respectively. Figure 4b shows the Nyquist plots of the two electrodes, which are used to estimate the effect of EO groups by charge-transfer resistance (R_{ct}). The electrode with PAA-PEG-Ca^{2+} binder exhibits lower R_{ct} (17.25 Ω) than that of PAA binder (29.87 Ω), which corresponds to the semicircle diameter of the intermediate-frequency region. The results indicate that the introduction of PEG can facilitate the transfer of Li ions.[50]

To further clarify the effect of the PAA-PEG-Ca^{2+} binder on maintaining Si-based anode integrity, scanning electron microscopy (SEM) was conducted to reveal the morphology change of Si electrodes with different polymer binders before and after cycling. At the pristine state, the thicknesses of the PAA-PEG-Ca^{2+}-SiNP, PAA-PEG-SiNP, and PAA-SiNP electrodes are 17.48, 17.88, and 16.66 μm, respectively, as shown in the cross-sectional SEM images in Figure 5a–c. After the 100th delithiation, the thicknesses increase to 26.42, 34.14, and 39.84 μm (Figure 5d–f), corresponding to the expansion of 51.1, 90.9, and 139.1%. This result demonstrates that the PAA-PEG-Ca^{2+} binder with a dual cross-linked network can buffer the volume change significantly compared with other polymer binders of PAA-PEG and PAA. Moreover, the structure of the SiNP electrode after cycling was shown in the top-view SEM images in Figure 5g–i. The PAA-PEG-Ca^{2+}-SiNP electrode reveals a relatively dense structure without obvious cracks, which has no noticeable difference with the initial fluffy flat morphology (Figures 5g and S6). In contrast, the PAA-PEG-SiNP and PAA-SiNP electrodes showed plenty of giant cracks with severe pulverization. Therefore, the electrode with the PAA-PEG-Ca^{2+} polymer binder embraces excellent mechanical properties to maintain Si-based anode integrity and guarantee tremendous cyclic performance.

Furthermore, the comparisons of electrochemical performances of Si anodes with different binders are summarized in Table 1. Compared with the linear PAA binder, the electrochemical performance of Si electrodes with the PAA-based single cross-linked binders has been significantly improved. However, the Si electrode with a 3D network PAA-PEG-Ca^{2+} binder displays the highest capacity retention (1596 mAh/g) at 2000 mA/g over 800 cycles than that of other binders. Compared to other double cross-linked binders, the silicon anodes with PAA-PEG-Ca^{2+} binder markedly enhance the capacity retention and cycle lifetime.

4. CONCLUSIONS

In summary, we have developed a water-soluble 3D polymer binder with a dual cross-linked network to address the issues caused by the volume expansion of Si. The abound of carboxyl groups provides strong adhesion with Si particles and Cu collector, improving the adhesion force and the integrity of the Si electrode. Combining chemical and physical cross-linking features by incorporating the soft segment of poly(ethylene glycol) and Ca^{2+} into PAA provided a stretchable 3D structure binder. It could efficiently mitigate Si anode's massive volume expansion during the cycling process, resulting in an excellent electrochemical cycling stability of the Si anode. Therefore, the current approach paves an avenue to settle the volume expansion concerns from large-capacity anode materials, such as silicon, phosphorous, and tin, to pursue high energy density.

■ ASSOCIATED CONTENT

Supporting Information

The Supporting Information is available free of charge at https://pubs.acs.org/doi/10.1021/acsaem.1c02231.

FTIR spectra of AA, PEG, PAA-PEG, and PAA-PEG-Ca^{2+}; BJH pore volume of Si particles; SEM image of Si particles; CV curves of the PAA-PEG-Ca^{2+}-SiNP, PAA-PEG-SiNP, and PAA-SiNP electrodes at a scanning rate of 0.05 mV/s; discharging capacity of electrodes with

https://doi.org/10.1021/acsaem.1c02231
ACS Appl. Energy Mater. XXXX, XXX, XXX−XXX

different ratios of PAA-PEG and Ca^{2+} binders when measured at 1.2 A/g; photograph and SEM images of Li metal and separator before and after cycles; and SEM image of the Si electrode before cycling (PDF)

AUTHOR INFORMATION

Corresponding Authors

Yangyang Feng − *State Key Laboratory for Mechanical Behavior of Materials, Shaanxi International Research Center for Soft Matter, Xi'an Jiaotong University, Xi'an 710049, China*; Email: fengyy@xjtu.edu.cn

Jiangxuan Song − *State Key Laboratory for Mechanical Behavior of Materials, Shaanxi International Research Center for Soft Matter, Xi'an Jiaotong University, Xi'an 710049, China*; orcid.org/0000-0001-6046-0760; Email: songjx@xjtu.edu.cn

Authors

Xingxing Jiao − *State Key Laboratory for Mechanical Behavior of Materials, Shaanxi International Research Center for Soft Matter, Xi'an Jiaotong University, Xi'an 710049, China*

Xiaodong Yuan − *State Key Laboratory for Mechanical Behavior of Materials, Shaanxi International Research Center for Soft Matter, Xi'an Jiaotong University, Xi'an 710049, China*

Jianqing Yin − *State Key Laboratory for Mechanical Behavior of Materials, Shaanxi International Research Center for Soft Matter, Xi'an Jiaotong University, Xi'an 710049, China*

Farshad Boorboor Ajdari − *Department of Applied Chemistry, Faculty of Chemistry, University of Kashan, Kashan 8731753153, Iran*

Guoxin Gao − *School of Chemistry, Xi'an Jiaotong University, Xi'an 710049, China*; orcid.org/0000-0002-1202-7281

Complete contact information is available at: https://pubs.acs.org/10.1021/acsaem.1c02231

Author Contributions

[‖]X.J. and X.Y. contributed equally to this work.

Notes

The authors declare no competing financial interest.

ACKNOWLEDGMENTS

This work is supported by the National Natural Science Foundation of China (Nos. 51602250 and 21875181), the Shaanxi Key Research and Development Project (No. 2019TSLGY07-05), and the 111 Project 2.0 (BP2018008). The authors thank Ren at the Instrument Analysis Center of Xi'an Jiaotong University for assisting with SEM analysis.

REFERENCES

(1) Dunn, B.; Kamath, H.; Tarascon, J.-M. Electrical Energy Storage for the Grid: A Battery of Choices. *Science* **2011**, *334*, 928−935.

(2) Armand, M.; Tarascon, J. M. Building better batteries. *Nature* **2008**, *451*, 652−657.

(3) Jiao, X. X.; Liu, Y. Y.; Li, B.; Zhang, W. X.; He, C.; Zhang, C. F.; Yu, Z. X.; Gao, T. Y.; Song, J. X. Amorphous phosphorus-carbon nanotube hybrid anode with ultralong cycle life and high-rate capability for lithium-ion batteries. *Carbon* **2019**, *148*, 518−524.

(4) Liu, Y.; Xu, X.; Jiao, X.; Guo, L.; Song, Z.; Xiong, S.; Song, J. LiXGe containing ion-conductive hybrid skin for high rate lithium metal anode. *Chem. Eng. J.* **2019**, *371*, 294−300.

(5) Jiao, X.; Liu, Y.; Li, T.; Zhang, C.; Xu, X.; Kapitanova, O. O.; He, C.; Li, B.; Xiong, S.; Song, J. Crumpled Nitrogen-Doped Graphene-Wrapped Phosphorus Composite as a Promising Anode for Lithium-Ion Batteries. *ACS Appl. Mater. Interfaces* **2019**, *11*, 30858−30864.

(6) Chen, H.; Ling, M.; Hencz, L.; Ling, H. Y.; Li, G.; Lin, Z.; Liu, G.; Zhang, S. Exploring Chemical, Mechanical, and Electrical Functionalities of Binders for Advanced Energy-Storage Devices. *Chem. Rev.* **2018**, *118*, 8936−8982.

(7) Song, J.; Li, X.; Zhang, J. G. Silicon-Based Anodes for Advanced Lithium-Ion Batteries. In *Encyclopedia of Inorganic and Bioinorganic Chemistry*; John Wiley & Sons, Ltd, 2019; pp 1−12.

(8) Kwon, T.-W.; Choi, J. W.; Coskun, A. The emerging era of supramolecular polymeric binders in silicon anodes. *Chem. Soc. Rev.* **2018**, *47*, 2145−2164.

(9) He, Y.; Xiang, K.; Zhou, W.; Zhu, Y.; Chen, X.; Chen, H. Folded-hand silicon/carbon three-dimensional networks as a binder-free advanced anode for high-performance lithium-ion batteries. *Chem. Eng. J.* **2018**, *353*, 666−678.

(10) Cho, Y.; Kim, J.; Elabd, A.; Choi, S.; Park, K.; Kwon, T. W.; Lee, J.; Char, K.; Coskun, A.; Choi, J. W. A Pyrene-Poly(acrylic acid)-Polyrotaxane Supramolecular Binder Network for High-Performance Silicon Negative Electrodes. *Adv. Mater.* **2019**, *31*, No. 1905048.

(11) Jiang, S.; Hu, B.; Shi, Z.; Chen, W.; Zhang, Z.; Zhang, L. Re-Engineering Poly(Acrylic Acid) Binder toward Optimized Electrochemical Performance for Silicon Lithium-Ion Batteries: Branching Architecture Leads to Balanced Properties of Polymeric Binders. *Adv. Funct. Mater.* **2019**, *30*, No. 1908558.

(12) Jeong, Y. K.; Choi, J. W. Mussel-Inspired Self-Healing Metallopolymers for Silicon Nanoparticle Anodes. *ACS Nano* **2019**, *13*, 8364−8373.

(13) Zhang, L.; Ding, Y.; Song, J. Crosslinked carboxymethyl cellulose-sodium borate hybrid binder for advanced silicon anodes in lithium-ion batteries. *Chin. Chem. Lett.* **2018**, *29*, 1773−1776.

(14) Manj, R. Z. A.; Zhang, F.; Ur Rehman, W.; Luo, W.; Yang, J. Toward understanding the interaction within Silicon-based anodes for stable lithium storage. *Chem. Eng. J.* **2020**, *385*, No. 123821.

(15) Qi, Y.; Wang, G.; Li, S.; Liu, T.; Qiu, J.; Li, H. Recent progress of structural designs of silicon for performance-enhanced lithium-ion batteries. *Chem. Eng. J.* **2020**, *397*, No. 125380.

(16) An, Y.; Fei, H.; Zeng, G.; Ci, L.; Xiong, S.; Feng, J.; Qian, Y. Green, Scalable, and Controllable Fabrication of Nanoporous Silicon from Commercial Alloy Precursors for High-Energy Lithium-Ion Batteries. *ACS Nano* **2018**, *12*, 4993−5002.

(17) An, Y.; Tian, Y.; Zhang, Y.; Wei, C.; Tan, L.; Zhang, C.; Cui, N.; Xiong, S.; Feng, J.; Qian, Y. Two-Dimensional Silicon/Carbon from Commercial Alloy and CO_2 for Lithium Storage and Flexible $Ti_3C_2T_x$ MXene-Based Lithium-Metal Batteries. *ACS Nano* **2020**, *14*, 17574−17588.

(18) Zhang, T.; Feng, Y.; Zhang, J.; He, C.; Itkis, D. M.; Song, J. Ultrahigh-rate sodium-ion battery anode enabled by vertically aligned (1T-2H MoS_2)/CoS_2 heteronanosheets. *Mater. Today Nano* **2020**, *12*, No. 100089.

(19) Liu, X. H.; Zhong, L.; Huang, S.; Mao, S. X.; Zhu, T.; Huang, J. Y. Size-Dependent Fracture of Silicon Nanoparticles During Lithiation. *ACS Nano* **2012**, *6*, 1522−1531.

(20) Wu, H.; Zheng, G.; Liu, N.; Carney, T. J.; Yang, Y.; Cui, Y. Engineering Empty Space between Si Nanoparticles for Lithium-Ion Battery Anodes. *Nano Lett.* **2012**, *12*, 904−909.

(21) Chae, C.; Noh, H. J.; Lee, J. K.; Scrosati, B.; Sun, Y. K. A High-Energy Li-Ion Battery Using a Silicon-Based Anode and a Nano-Structured Layered Composite Cathode. *Adv. Funct. Mater.* **2014**, *24*, 3036−3042.

(22) Wu, Y.-J.; Chen, Y.-A.; Huang, C.-L.; Su, J.-T.; Hsieh, C.-T.; Lu, S.-Y. Small highly mesoporous silicon nanoparticles for high performance lithium ion based energy storage. *Chem. Eng. J.* **2020**, *400*, No. 125958.

(23) Liu, X. H.; Zhang, L. Q.; Zhong, L.; Liu, Y.; Zheng, H.; Wang, J. W.; Cho, J.-H.; Dayeh, S. A.; Picraux, S. T.; Sullivan, J. P.; et al.

Ultrafast electrochemical lithiation of individual Si nanowire anodes. *Nano Lett.* **2011**, *11*, 2251−2258.
(24) Cui, L.-F.; Ruffo, R.; Chan, C. K.; Peng, H.; Cui, Y. Crystalline-Amorphous Core−Shell Silicon Nanowires for High Capacity and High Current Battery Electrodes. *Nano Lett.* **2009**, *9*, 491−495.
(25) Park, M.-H.; Kim, M. G.; Joo, J.; Kim, K.; Kim, J.; Ahn, S.; Cui, Y.; Cho, J. Silicon Nanotube Battery Anodes. *Nano Lett.* **2009**, *9*, 3844−3847.
(26) Song, T.; Xia, J.; Lee, J.-H.; Lee, D. H.; Kwon, M.-S.; Choi, J.-M.; Wu, J.; Doo, S. K.; Chang, H.; Park, W. I.; Zang, D. S.; Kim, H.; Huang, Y.; Hwang, K.-C.; Rogers, J. A.; Paik, U. Arrays of Sealed Silicon Nanotubes As Anodes for Lithium Ion Batteries. *Nano Lett.* **2010**, *10*, 1710−1716.
(27) Abel, P. R.; Lin, Y.-M.; Celio, H.; Heller, A.; Mullins, C. B. Improving the Stability of Nanostructured Silicon Thin Film Lithium-Ion Battery Anodes through Their Controlled Oxidation. *ACS Nano* **2012**, *6*, 2506−2516.
(28) Datta, M. K.; Maranchi, J.; Chung, S. J.; Epur, R.; Kadakia, K.; Jampani, P.; Kumta, P. N. Amorphous silicon-carbon based nano-scale thin film anode materials for lithium ion batteries. *Electrochim. Acta* **2011**, *56*, 4717−4723.
(29) Li, X.; Gu, M.; Hu, S.; Kennard, R.; Yan, P.; Chen, X.; Wang, C.; Sailor, M. J.; Zhang, J. G.; Liu, J. Mesoporous silicon sponge as an anti-pulverization structure for high-performance lithium-ion battery anodes. *Nat. Commun.* **2014**, *5*, No. 4105.
(30) Tao, H. C.; Fan, L. Z.; Qu, X. Facile synthesis of ordered porous Si@ C nanorods as anode materials for Li-ion batteries. *Electrochim. Acta* **2012**, *71*, 194−200.
(31) Li, X.; Meduri, P.; Chen, X.; Qi, W.; Engelhard, M. H.; Xu, W.; Ding, F.; Xiao, J.; Wang, W.; Wang, C.; Zhang, J.-G.; Liu, J. Hollow core-shell structured porous Si-C nanocomposites for Li-ion battery anodes. *J. Mater. Chem.* **2012**, *22*, 11014−11017.
(32) Chen, S.; Gordin, M. L.; Yi, R.; Howlett, G.; Sohn, H.; Wang, D. Silicon core-hollow carbon shell nanocomposites with tunable buffer voids for high capacity anodes of lithium-ion batteries. *Phys. Chem. Chem. Phys.* **2012**, *14*, 12741−12745.
(33) Liu, N.; Wu, H.; McDowell, M. T.; Yao, Y.; Wang, C.; Cui, Y. A Yolk-Shell Design for Stabilized and Scalable Li-Ion Battery Alloy Anodes. *Nano Lett.* **2012**, *12*, 3315−3321.
(34) Chen, Z.; Wang, C.; Lopez, J.; Lu, Z. D.; Cui, Y.; Bao, Z. A. High-Areal-Capacity Silicon Electrodes with Low-Cost Silicon Particles Based on Spatial Control of Self-Healing Binder. *Adv. Energy Mater.* **2015**, *5*, No. 1401826.
(35) Munaoka, T.; Yan, X. Z.; Lopez, J.; To, J. W. F.; Park, J.; Tok, J. B. H.; Cui, Y.; Bao, Z. N. Ionically Conductive Self-Healing Binder for Low Cost Si Microparticles Anodes in Li-Ion Batteries. *Adv. Energy Mater.* **2018**, *8*, No. 1703138.
(36) Choi, S.; Kwon, T. W.; Coskun, A.; Choi, J. W. Highly elastic binders integrating polyrotaxanes for silicon microparticle anodes in lithium ion batteries. *Science* **2017**, *357*, 279−283.
(37) Wang, L.; Liu, T.; Peng, X.; Zeng, W.; Jin, Z.; Tian, W.; Gao, B.; Zhou, Y.; Chu, P. K.; Huo, K. Highly Stretchable Conductive Glue for High-Performance Silicon Anodes in Advanced Lithium-Ion Batteries. *Adv. Funct. Mater.* **2018**, *28*, No. 1704858.
(38) Magasinski, A.; Zdyrko, B.; Kovalenko, I.; Hertzberg, B.; Burtovyy, R.; Huebner, C. F.; Fuller, T. F.; Luzinov, I.; Yushin, G. Toward Efficient Binders for Li-Ion Battery Si-Based Anodes: Polyacrylic Acid. *ACS Appl. Mater. Interfaces* **2010**, *2*, 3004−3010.
(39) Huang, C. Influence of molecular structure of Carboxymethyl Cellulose on High Performance Silicon Anode in Lithium-Ion Batteries. *Int. J. Electrochem. Sci.* **2019**, 4799−4811.
(40) Jiao, X.; Yin, J.; Xu, X.; Wang, J.; Liu, Y.; Xiong, S.; Zhang, Q.; Song, J. Highly Energy-Dissipative, Fast Self-Healing Binder for Stable Si Anode in Lithium-Ion Batteries. *Adv. Funct. Mater.* **2021**, *31*, No. 2005699.
(41) Zhang, L.; Jiao, X. X.; Feng, Z. H.; Li, B.; Feng, Y. Y.; Song, J. X. A nature-inspired binder with three-dimensional cross-linked networks for silicon-based anodes in lithium-ion batteries. *J. Power Sources* **2021**, *484*, No. 229198.
(42) Hu, L.; Zhang, X.; Li, B.; Jin, M.; Shen, X.; Luo, Z.; Tian, Z.; Yuan, L.; Deng, J.; Dai, Z.; Song, J. Design of high-energy-dissipation, deformable binder for high-areal-capacity silicon anode in lithium-ion batteries. *Chem. Eng. J.* **2021**, *420*, No. 129991.
(43) Jin, M.; Li, B.; Hu, L.; Zhao, P.; Zhang, Q.; Song, J. Functional copolymer binder for nickel-rich cathode with exceptional cycling stability at high temperature through coordination interaction. *J. Energy Chem.* **2021**, *60*, 156−161.
(44) Song, J.; Zhou, M.; Yi, R.; Xu, T.; Gordin, M. L.; Tang, D.; Yu, Z.; Regula, M.; Wang, D. Interpenetrated Gel Polymer Binder for High-Performance Silicon Anodes in Lithium-ion Batteries. *Adv. Funct. Mater.* **2014**, *24*, 5904−5910.
(45) Liu, T. F.; Chu, Q. L.; Yan, C.; Zhang, S. Q.; Lin, Z.; Lu, J. Interweaving 3D Network Binder for High-Areal-Capacity Si Anode through Combined Hard and Soft Polymers. *Adv. Energy Mater.* **2019**, *9*, No. 1802645.
(46) Cao, P. F.; Yang, G.; Li, B. R.; Zhang, Y. M.; Zhao, S.; Zhang, S.; Erwin, A.; Zhang, Z. C.; Sokolov, A. P.; Nanda, J.; Saito, T. Rational Design of a Multifunctional Binder for High-Capacity Silicon-Based Anodes. *ACS Energy Lett.* **2019**, *4*, 1171−1180.
(47) Xu, Z.; Yang, J.; Zhang, T.; Nuli, Y.; Wang, J.; Hirano, S.-I. Silicon Microparticle Anodes with Self-Healing Multiple Network Binder. *Joule* **2018**, *2*, 950−961.
(48) Li, Z. H.; Zhang, Y. P.; Liu, T. F.; Gao, X. H.; Li, S. Y.; Ling, M.; Liang, C. D.; Zheng, J. C.; Lin, Z. Silicon Anode with High Initial Coulombic Efficiency by Modulated Trifunctional Binder for High-Areal-Capacity Lithium-Ion Batteries. *Adv. Energy Mater.* **2020**, *10*, No. 1903110.
(49) Tang, R.; Ma, L.; Zhang, Y.; Zheng, X.; Shi, Y.; Zeng, X.; Wang, X.; Wei, L. A Flexible and Conductive Binder with Strong Adhesion for High Performance Silicon-Based Lithium-Ion Battery Anode. *ChemElectroChem* **2020**, *7*, 1992−2000.
(50) Zeng, W. W.; Wang, L.; Peng, X.; Liu, T. F.; Jiang, Y. Y.; Qin, F.; Hu, L.; Chu, P. K.; Huo, K. F.; Zhou, Y. H. Enhanced Ion Conductivity in Conducting Polymer Binder for High-Performance Silicon Anodes in Advanced Lithium-Ion Batteries. *Adv. Energy Mater.* **2018**, *8*, No. 1702314.
(51) Zhu, L.; Du, F.; Zhuang, Y.; Dai, H.; Cao, H.; Adkins, J.; Zhou, Q.; Zheng, J. Effect of crosslinking binders on Li-storage behavior of silicon particles as anodes for lithium ion batteries. *J. Electroanal. Chem.* **2019**, *845*, 22−30.
(52) Gao, Y.; Qiu, X.; Wang, X.; Gu, A.; Zhang, L.; Chen, X.; Li, J.; Yu, Z. Chitosan-g-Poly(acrylic acid) Copolymer and Its Sodium Salt as Stabilized Aqueous Binders for Silicon Anodes in Lithium-Ion Batteries. *ACS Sustainable Chem. Eng.* **2019**, *7*, 16274−16283.
(53) Koo, B.; Kim, H.; Cho, Y.; Lee, K. T.; Choi, N.-S.; Cho, J. A Highly Cross-Linked Polymeric Binder for High-Performance Silicon Negative Electrodes in Lithium Ion Batteries. *Angew. Chem., Int. Ed.* **2012**, *51*, 8762−8767.
(54) Hwang, C.; Joo, S.; Kang, N. R.; Lee, U.; Kim, T. H.; Jeon, Y.; Kim, J.; Kim, Y. J.; Kim, J. Y.; Kwak, S. K.; Song, H. K. Breathing silicon anodes for durable high-power operations. *Sci. Rep.* **2015**, *5*, No. 14433.
(55) Wei, L.; Chen, C.; Hou, Z.; Wei, H. Poly (acrylic acid sodium) grafted carboxymethyl cellulose as a high performance polymer binder for silicon anode in lithium ion batteries. *Sci. Rep.* **2016**, *6*, No. 19583.
(56) Lim, S.; Lee, K.; Shin, I.; Tron, A.; Mun, J.; Yim, T.; Kim, T.-H. Physically cross-linked polymer binder based on poly(acrylic acid) and ion-conducting poly(ethylene glycol-co-benzimidazole) for silicon anodes. *J. Power Sources* **2017**, *360*, 585−592.
(57) Lü, L.; Lou, H.; Xiao, Y.; Zhang, G.; Wang, C.; Deng, Y. Synthesis of triblock copolymer polydopamine-polyacrylic-polyoxyethylene with excellent performance as a binder for silicon anode lithium-ion batteries. *RSC Adv.* **2018**, *8*, 4604−4609.
(58) Wu, Z.-H.; Yang, J.-Y.; Yu, B.; Shi, B.-M.; Zhao, C.-R.; Yu, Z.-L. Self-healing alginate−carboxymethyl chitosan porous scaffold as an effective binder for silicon anodes in lithium-ion batteries. *Rare Met.* **2019**, *38*, 832−839.

https://doi.org/10.1021/acsaem.1c02231
ACS Appl. Energy Mater. XXXX, XXX, XXX−XXX

(59) Kwon, T. W.; Jeong, Y. K.; Deniz, E.; AlQaradawi, S. Y.; Choi, J. W.; Coskun, A. Dynamic Cross-Linking of Polymeric Binders Based on Host-Guest Interactions for Silicon Anodes in Lithium Ion Batteries. *ACS Nano* **2015**, *9*, 11317−11324.

https://doi.org/10.1021/acsaem.1c02231
ACS Appl. Energy Mater. XXXX, XXX, XXX−XXX